Interplay of electron-electron and electron-phonon interactions in the low-temperature phase of $1T$-TaS_2

Doohee Cho,[1] Yong-Heum Cho,[2,3] Sang-Wook Cheong,[3,4] Ki-Seok Kim,[2] and Han Woong Yeom[1,2,*]

[1]*Center for Artificial Low Dimensional Electronic Systems, Institute for Basic Science (IBS), 77 Cheongam-Ro, Pohang 790-784, Republic of Korea*

[2]*Department of Physics, Pohang University of Science and Technology (POSTECH), Pohang 790-784, Republic of Korea*

[3]*Laboratory for Pohang Emergent Materials, Pohang University of Science and Technology, Pohang 790-784, Korea*

[4]*Rutgers Center for Emergent Materials and Department of Physics and Astronomy, Rutgers University, Piscataway, New Jersey 08854, USA*

(Received 2 December 2014; published 18 August 2015)

We investigate the interplay of the electron-electron and electron-phonon interactions in the electronic structure of an exotic insulating state in the layered dichalcogenide $1T$-TaS_2, where the charge-density-wave (CDW) order coexists with a Mott correlation gap. Scanning tunneling microscopy and spectroscopy measurements with high spatial and energy resolution determine unambiguously the CDW and the Mott gap as 0.20–0.24 eV and 0.32 eV, respectively, through the real space electron phases measured across the multiply formed energy gaps. An unusual local reduction of the Mott gap is observed on the defect site, which indicates the renormalization of the on-site Coulomb interaction by the electron-phonon coupling as predicted by the Hubbard-Holstein model. The Mott-gap renormalization provides insight into the disorder-induced quasimetallic phases of $1T$-TaS_2.

DOI: 10.1103/PhysRevB.92.085132 PACS number(s): 71.10.Hf, 71.20.Be, 71.27.+a, 71.30.+h

I. INTRODUCTION

Metal-insulator transitions in low dimensional condensed matter systems are driven by various interactions between relevant degrees of freedom, such as spin, charge, orbital, and lattice. For example, charge density waves (CDW) [1] and Mott insulators [2] are paradigmatic examples of electron-phonon (*e-ph*) and electron-electron (*e-e*) couplings, respectively. These couplings are often entangled to yield exotic states of electrons as recently discussed for high-temperature superconductors [3]. On the other hand, the interplay of *e-ph* and *e-e* couplings has been discussed for a while for the CDW transition [4] in a layered transition metal dichalcogenide of $1T$-TaS_2 [5]. Upon decreasing temperature, it undergoes a series of transitions from a metallic phase through incommensurate and nearly commensurate CDW to commensurate (C)-CDW [4]. The ordered CDW superstructures could be directly observed using scanning tunneling microscopy (STM) in real space [6,7]. The C-CDW superstructure splits the broad metallic band into a manifold of narrow subbands but cannot account for the most important gap opening at the Fermi level (E_F) with one half-filled band left [8]. The insulating gap was then explained by introducing the on-site Coulomb repulsion, which is enhanced by the substantial narrowing of the band width due to the CDW formation [5]. Thus, the multiple gap structure in this system itself is a hallmark of the interplay between *e-ph* and *e-e* couplings.

However, while this material has been investigated for a long time, the multiple gap structure is not fully characterized yet by experiments. The gap structure was investigated by angle resolved photoemission spectroscopy (ARPES) [9], inverse ARPES [10], and scanning tunneling spectroscopy (STS) [7] below the critical temperature ($T_c \sim 180$ K). ARPES probed only the occupied part of the gap and inverse ARPES for the empty part did not provide proper energy resolution. The previous STS study only focused on the gap at E_F without any clear information on the multiple gaps. Moreover, these spectroscopic works reported substantially larger gaps than those measured by optical and transport measurements [11–13]. Considering the fact that the multiple gap structure is crucially important to understand not only the ground state but also the statically or dynamically excited states with the anomalous metallic property and the superconductivity of this system [14–18], the experimental establishment of the energy gap structure in its ground state is imperative. It is also important to trace how the Mott or CDW gap changes upon external perturbations or internal fluctuations in this respect. Moreover, generally speaking, beyond the gap structure, little is known about the physical consequences of the coupled *e-e* and *e-ph* interactions in this interesting system.

In this Letter, we report the STS results with substantially improved resolution, which identifies and quantifies clearly the multiple gaps. The origins of different gaps are unambiguously determined by the real space phases of relevant electrons. Furthermore, we unveil the local reduction of the Mott gap at the defect site, which is presumably renormalized by the local variation of the *e-ph* coupling. This manifests the interplay of *e-ph* and *e-e* couplings within the Hubbard-Holstein model and has important implications for the emergence of intriguing metallic C-CDW phases with intrinsic or extrinsic disorders [17,19].

II. EXPERIMENT

We performed STM and STS measurements with an ultrahigh vacuum cryogenic STM (Unisoku, Japan) at 78 K. The real space electron density as a function of energy was acquired via spatially resolved (SR) differential conductance (dI/dV) measurements; the normalized tunneling conductance $[(dI/dV)/(I/V)]$ is proportional to the local density of states (LDOS) [20]. The lock-in technique with a bias modulation of $V_{rms} = 20$ mV, $f = 1$ kHz was applied to acquire dI/dV.

*yeom@postech.ac.kr

$1T$-TaS_2 single crystals were grown by the chemical vapor transport method with iodine as a transport agent. The crystals were cleaved in high vacuum before cooling down.

III. RESULTS AND DISCUSSION

Below the transition temperature of ~180 K, the CDW forms a long-range ordered superstructure [7,9] as shown in the STM topographic image of Fig. 1(a). Its Fourier transformation [the inset of Fig. 1(a)] shows strong peaks and their higher orders with a wavelength of $\sqrt{13}a_0 \sim 12.1$ Å, which are rotated counterclockwise by 13.9° with respect to the 1×1 lattice of $1T$-TaS_2. The zoom-in image of Fig. 1(b) shows how the CDW maxima match with the underlaying Ta lattice. The lattice is distorted into the unit of 13 Ta atoms with 12 atoms in the shape of a star of David displaced toward the center atom.

In order to detail the electronic structure of the C-CDW phase, SR-STS measurements were performed simultaneously with the topographic imaging of Fig. 1(b). A particular line scan along the green arrow in Fig. 1(b) is shown in Fig. 2(a) and a few typical normalized conductance curves in Fig. 2(b) [21]. The opening of the energy gap close to E_F is clearly resolved. A gap size is unambiguously determined by the LDOS peaks at +0.22 and –0.10 eV as 0.32 eV. They would correspond to the upper and lower Hubbard states [U(L)HS]. More clear evidence of the Mott gap will be discussed below. Depending on samples and tip conditions, the positions of prominent peaks vary within a few tens of meV [7]. This can be related with the spatial inhomogeneity of the doping level induced by intrinsic defects. However, the size of the correlation gap is consistent with 320 meV and E_F is always closer to the LHS. In addition to the gap at E_F, three other gaplike features are identified around +0.30, –0.25, and –0.65 eV (marked by arrows in Fig. 2), which divide the measured spectra into five subbands. The correlation gap and the other gaplike features are all washed away at room temperature as shown in Fig. 2(b) exhibiting their clear temperature dependence [22].

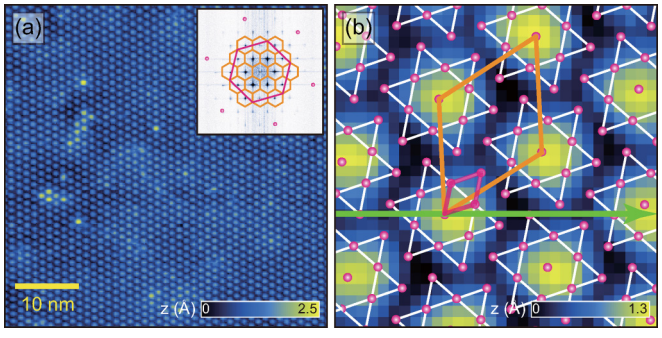

FIG. 1. (Color online) (a) STM image (tunneling current I_t = 100 pA, sample bias $V_s = +0.2$ V and 50×50 nm^2) of $1T$-TaS_2 at 78 K displaying long-range ordered CDWs. The inset shows its corresponding 2D Fourier transform. Orange and purple hexagons [parallelograms in Fig. 1(b)] indicate the first Brillouin zone (unit cells in real space) of $p(\sqrt{13} \times \sqrt{13})$R13.9° C-CDW and 1×1 normal states, respectively. (b) STM image (3.5×3.5 nm^2 and 30×30 pixel) acquired during dI/dV measurements ($I_t = 100$ pA and $V_S = -1.20$ V). The superimposed sketches highlight the units of the CDW.

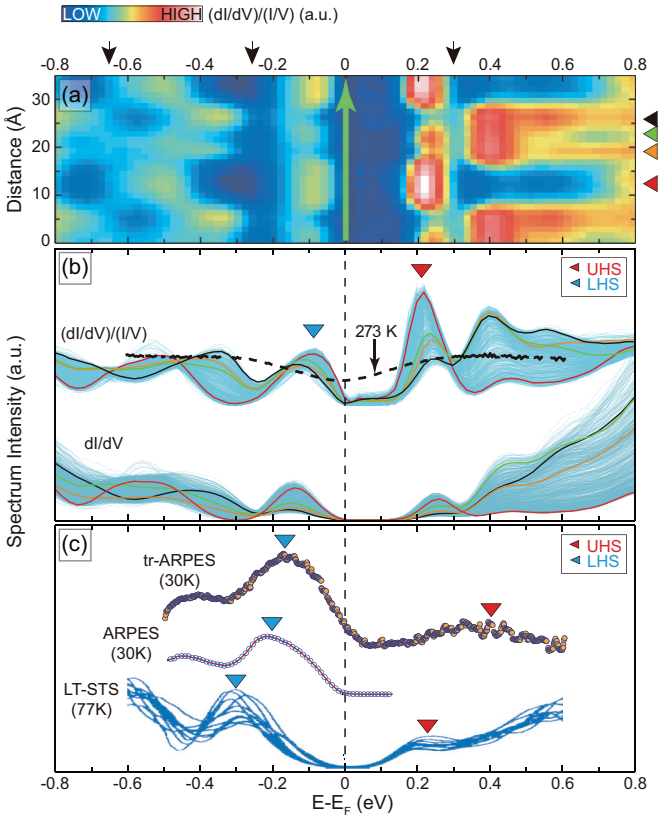

FIG. 2. (Color) (a) Normalized dI/dV spectrum acquired along the green arrow in Fig. 1(b). (b) A collection of 900 normalized dI/dV (upper part) and raw dI/dV (lower part) spectra over the area shown in Fig. 1(b). The highlighted spectra (red, orange, green, and black) are obtained at the marked positions in Fig. 2(a). The black dashed curve was acquired at 273 K. (c) Previously reported spectra, acquired by STS [7], ARPES, and tr-ARPES [23] for the C-CDW phase. The red (blue) triangle indicates the U(L)HS.

The previous spectroscopic results summarized in Fig. 2(c) consistently indicated the insulating property of the C-CDW phase of $1T$-TaS_2 [7,23]. However, the estimated gap size ranges from 500 to 600 meV, which is substantially larger than the present result. This variation can stem largely from experimental limitations in the energy range or the resolution. Considering the broad line shape and the limited resolution, the ARPES results [9,23,24] seem roughly consistent with the present results for the LHS. The even more limited resolution and sensitivity are likely to prevent properly identifying the UHS in the inverse ARPES [10] and time-resolved ARPES works [23]. The line shape of the very early STS measurement suggests that it could not resolve the first and the second peak of filled states in our STS spectra [7]. The suppression of the spectral intensity near E_F, especially for the LHS peak, is noticeable in the previous measurement, which is highly possible for a low conductance tip condition. Furthermore, this pioneering work did not address the multiple gap structure discussed in the following. On the other hand the optical conductivity works measured a much smaller band gap of 100–200 meV [11,13]. If one considers the finite spectral width of the U(L)HS peak in STS, the present measurement agrees very well with this measurement, establishing firmly

the standard for the Mott gap of this material. The quantitative calculations taking into account of the correlation effect consistently reproduced the gap size of about 200 meV with the on-site Coulomb energy of 2–4 eV [25,26].

As mentioned above, in addition to the Mott gap at E_F, we found a few other gaplike features and their distinct characteristics can be shown clearly through the real space phase of associated electrons. Since CDW gaps of two-dimensional (2D) CDW systems usually have the momentum dependence, momentum-integrated STS spectra often do not show a clear zero conductance energy gap especially when the gap is away from E_F, making the identification of CDW gaps difficult [27]. However, the phase flip of the real space electron density is expected across any band gap formed by a periodic lattice distortion [27–31] and thus can be a sign of the presence of a CDW-induced gap in contrast to the Mott gap.

The CDW gaps in 1T-TaS_2 do not show the zero but the reduced LDOS intensity. We can attribute the clear dip features in the spatially averaged spectrum as possible energy gap positions [indicated by black dots in Fig. 3(a)]. Across these LDOS dips, the subband onsets can be assigned by shoulder- or peaklike features [black arrows in Fig. 3(a)] in spectra. They are most clearly resolved in the spatially resolved spectra as shown in Fig. 3(a) or Fig. 2(a). In order to quantify the phase difference across these LDOS dips, for example, between two states α_{ij} and β_{ij}, we use the normalized correlation coefficient (NCC) between two corresponding images, NCC=$\langle(\alpha_{ij}-\mu_\alpha)(\beta_{ij}-\mu_\beta)\rangle/(\sigma_\alpha\sigma_\beta)$, where μ and σ are averages and standard deviations of the images [32]. The spatially averaged STS spectrum in Fig. 3(a) was colored with the value of NCC obtained, showing how the relative real space phase changes for different electronic states. One can confirm that the real space phases at the subband onset across the presumed gaps are flipped as expected [Fig. 3(b)]. We note that this quantitative analysis can in principle be affected by the tunneling junction itself, that is, the tunneling bias and current condition. However, the phase flips are consistently observed with a few different tunneling conditions in the STS measurements as partly shown in Fig. 5(c). Note that the CDW gap positions in the energy agree well with the previous band structure calculations [8,33] and the ARPES measurements [9,24,34]. As a result, we can quantify the gap sizes as 0.22 ± 0.02 eV; three CDW gaps, two in the occupied and the other in the unoccupied states, have a similar size. This manifests further the common origin of these gaps, the periodic potential provided by CDW and the lattice distortion. The reported gap sizes in filled states of 100–150 meV and 100–200 meV [8,9,24,33,34], respectively, are in reasonable agreement with the present quantification.

Beyond the distinct character of the Mott and CDW gaps, the real space electron densities of UHS and LHS show the clear particle-hole asymmetry; the former is more localized at the center Ta atom than the latter [Fig. 3(b)]. This wave function characteristic seems consistent with the STS spectra where the UHS has a narrower bandwidth (larger spectral peak intensity) than the LHS. This asymmetry in 1T-TaS_2 has not been reported so far in this system and its origin is not clear at this point.

For disordered 1T-TaS_2, intriguing metallic behaviors were reported previously [24,35]. This metallic state was explained

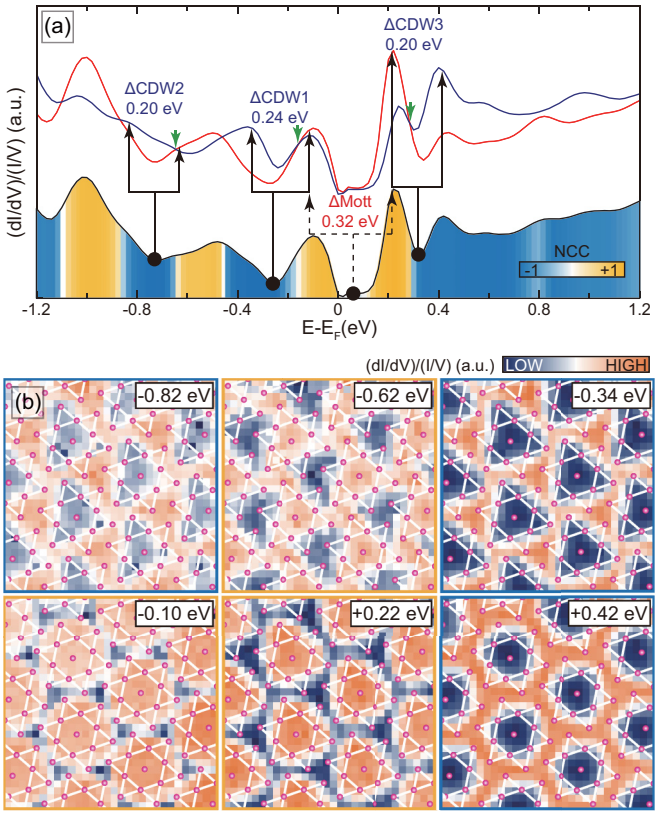

FIG. 3. (Color online) (a) Spatially averaged STS spectrum. The color scale indicates the normalized correlation coefficient (NCC) as referenced by the image at +0.22 eV. The red and blue curves are also averaged spectra which are acquired in the enhanced and suppressed region in the LDOS map of the UHS, respectively. The black dots denote the reductions of the LDOS intensity due to the gap opening. The black arrows mark the subband onsets (shoulders or peaks) close to the dips. The green arrows indicate the phase flip between the onsets. (b) LDOS maps of the states marked with arrows in Fig. 3(a) on a 3.5 ×3.5 nm^2 area. The frame colors of the maps represent their NCC.

by the screening of the e-e Coulomb interaction through charge carriers of the discommensurations induced by the defects. This sounds similar to the nearly commensurate CDW phase found at higher temperatures. Note that the effect of disorders on the conductivity of a correlated system can also be influenced by the aforementioned particle-hole asymmetry in theory [36]. More importantly, no direct and clear spectroscopic information is available on how a defect affects the correlation effect.

As shown in Figs. 4(a) and 4(b), the intrinsic defects do not destroy the long-range CDW ordering at all but lead only to a modification of the electronic structure in a single CDW maximum. There are two kinds of major defects. Their populations are comparable to each other. They exhibit the moderately (type A) and the strongly deformed feature (type B) from pristine CDW clusters [Fig. 4(c)]. The difference between these two different types are even more clear in their spectra shown in Fig. 4(d). As expected from the STM image, the type B defect shows strong modification of the spectra from that of a pristine CDW cluster, which is manifested by the appearance

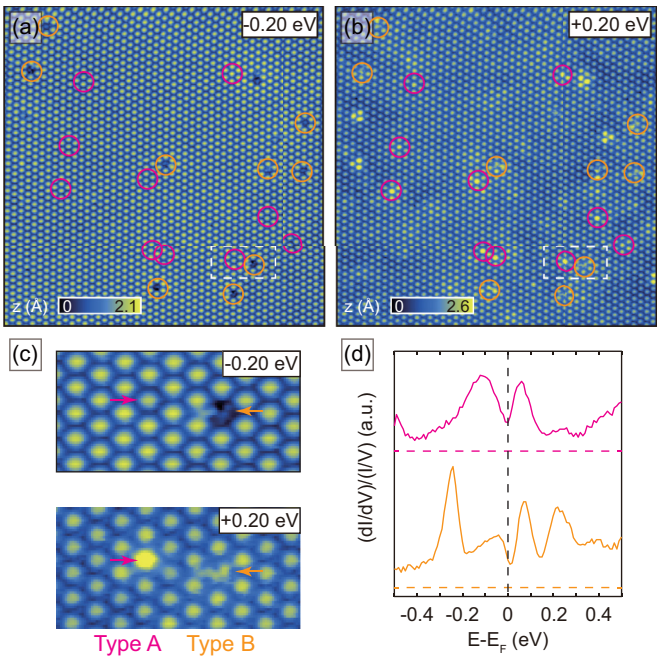

FIG. 4. (Color online) Filled (a) and empty (b) state STM images (I_t = 100 pA, $V_s = \mp$ 0.20 eV, and 52 ×52 nm^2) of the 1T-TaS$_2$ surface with point defects marked by the circles. (c) The enlarged STM images of two types of defects marked by dashed boxes in Figs. 4(a) and 4(b). (d) Normalized dI/dV spectra of two different defect types. The colors of the circles in the STM image and the spectra indicate their types.

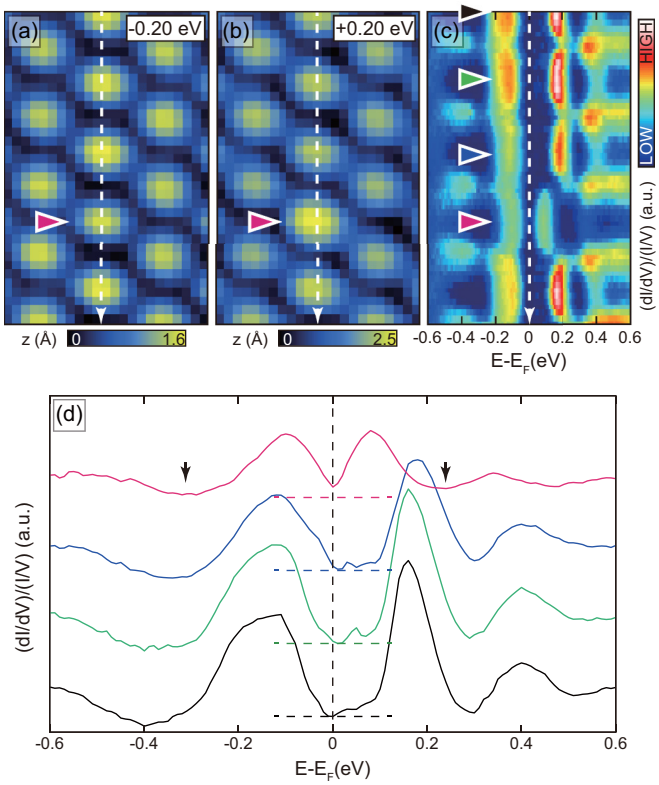

FIG. 5. (Color online) Filled (a) and empty (b) state STM images (I_t = 100 pA, $V_s = \mp$ 0.20 eV and 3.5 ×5.5 nm^2) of type-A defect on the 1T-TaS$_2$ surface, marked by the triangles. (c) Normalized differential conductance map measured along the white dashed arrow in Figs. 5(a) and 5(b). The tunneling conditions are I_t = 300 pA and V_S = –0.80 V. (d) Representative normalized dI/dV spectra acquired at the CDW crests denoted by triangles in Fig. 5(c). The black arrows indicate the subband splittings which are similar to the pristine CDW clusters.

of strong LDOS peaks at ± 0.25 eV. For the understanding of the spectral modification, we need to characterize the atomic structure of the defect, which is beyond the scope of the present work. In contrast, the spectrum of a type-A defect [a magenta curve in Fig. 4(d)] is very much consistent with that of a pristine CDW cluster exhibiting only the reduction of the Mott gap without any additional spectral feature. Our spatially resolved STS results directly show the difference of the electronic structure between the type-A defect and neighboring pristine CDW clusters. We acquired normalized dI/dV curves cross the defects along the white dashed arrows in Figs. 5(a) and 5(b). As shown in the LDOS map as a function of energy and position [Fig. 5(c)], the correlation gap is reduced from 320 to 180 meV. Especially, the other gap features driven by CDW reconstruction are preserved at the center of the defect. This implies that the type-A defect does not destroy the half-filled condition. Hence, we need the other factor to explain the renormalization of the correlation strength.

The local reduction of the Mott gap has never been reported previously and is sharply contrasting with the known behavior of dopants in a conventional Mott insulator; the spectral weight of the U(L)HS is transferred partially to an adjacent gap state [37]. Since doping generates a metal-insulator transition and superconductivity in strongly correlated electron systems, the effect of the dopants has been intensively studied so far [38]. The recent STS results of electron-doped transition-metal oxide Mott insulators, known as conventional correlated systems, exhibit the shoulderlike feature close to UHS without a remarkable change of the correlated gap size [39,40]. The spatially localized in-gap state was well reproduced by theoretical calculations [41].

However, the reduction of the gap size can be explained by the other aspect of the interplay between *e-e* and *e-ph* couplings within the Hubbard-Hostein model. In this model, the effective *e-e* coupling is renormalized by the interaction between electrons and optical phonons as given by $U_{\text{eff}} = U_{e-e} - 2g^2/\omega_0$ (ω_0 denotes the optical phonon frequency and g the *e-ph* coupling constant) [42]. The previous optical conductance measurements evidenced the optical phonons at the relevant energy range of 25 meV, which also exhibit the temperature-dependent softening [13]. This strongly suggests that the optical phonons can also be tuned by the local structural deformations. Our scenario is that the defect-induced local structural deformation reduces the optical phonon frequency and in turn leads to the reduced effective interaction U_{eff}. The reduced U_{eff} would make the Mott gap smaller and the finite width of the U(L)HS drives the system marginally metallic as shown in Fig. 5. This result bears important implications for the appearance of the quasimetallic behavior in the C-CDW phase of disordered 1T-TaS$_2$ [17,19].

IV. CONCLUSION

In summary, we have demonstrated the interplay between *e-ph* and *e-e* coupling in the electronic structure of the low-temperature ground state of 1*T*-TaS_2 using spatially resolved scanning tunneling spectroscopy. The multiple gap structure consisting of Mott and CDW gaps, the primary hallmark of the interplay, is well quantified and its distinct origins are unambiguously visualized through the real space phases of the relevant electrons. The defect-induced local reduction of the Mott gap is revealed and interpreted to reflect the effect of the local *e-ph* interaction within the Hubbard-Holstein model, which is another hallmark of the interplay.

ACKNOWLEDGMENTS

This work was supported by Institute for Basic Science (Grant No. IBS-R015-D1). Y.H.C. and S.W.C. are partially supported by the Max Planck POSTECH/KOREA Research Initiative Program (Grant No. 2011-0031558) through NRF of Korea funded by MEST.

[1] G. Grüner, Rev. Mod. Phys. **60**, 1129 (1988).
[2] N. Mott, Rev. Mod. Phys. **40**, 677 (1968).
[3] Lauren E. Hayward *et al.*, Science **343**, 1336 (2014).
[4] J. A. Wilson, F. Di Salvo, and S. Mahajan, Adv. Phys. **24**, 117 (1975).
[5] P. Fazekas and E. Tosatti, Philos. Mag. B **39**, 229 (1979).
[6] X. L. Wu and C. M. Lieber, Phys. Rev. Lett. **64**, 1150 (1990).
[7] J.-J. Kim, W. Yamaguchi, T. Hasegawa, and K. Kitazawa, Phys. Rev. Lett. **73**, 2103 (1994).
[8] N. Smith, S. Kevan, and F. DiSalvo, J. Phys. C: Solid State Phys. **18**, 3175 (1985).
[9] F. Clerc, C. Battaglia, M. Bovet, L. Despont, C. Monney, H. Cercellier, M. G. Garnier, P. Aebi, H. Berger, and L Forró, Phys. Rev. B **74**, 155114 (2006).
[10] H. Sato, M. Arita, Y. Utsumi, Y. Mukaegawa, M. Sasaki, A. Ohnishi, M. Kitaura, H. Namatame, and M. Taniguchi, Phys. Rev. B **89**, 155137 (2014).
[11] A. Barker, Jr, J. Ditzenberger, and F. DiSalvo, Phys. Rev. B **12**, 2049 (1975).
[12] N. Kobayashi and Y. Muto, Solid State Commun. **30**, 337 (1979).
[13] L. V. Gasparov, K. G. Brown, A. C. Wint, D. B. Tanner, H. Berger, G. Margaritondo, R. Gaál, and L. Forró, Phys. Rev. B **66**, 094301 (2002).
[14] B. Sipos *et al.*, Nat. Mater. **7**, 960 (2008).
[15] R. Ang, Y. Tanaka, E. Ieki, K. Nakayama, T. Sato, L. J. Li, W. J. Lu, Y. P. Sun, and T. Takahashi, Phys. Rev. Lett. **109**, 176403 (2012).
[16] R. Ang, Y. Miyata, E. Ieki, K. Nakayama, T. Sato, Y. Liu, W. J. Lu, Y. P. Sun, and T. Takahashi, Phys. Rev. B **88**, 115145 (2013).
[17] E. Lahoud, O. N. Meetei, K. B. Chaska, A. Kanigel, and N. E. Trivedi, Phys. Rev. Lett. **112**, 206402 (2014).
[18] L. Stojchevska *et al.*, Science **344**, 177 (2014).
[19] T. Isa *et al.*, J. Low Temp. Phys. **127**, 63 (2002).
[20] C. J. Chen, *Introduction to Scanning Tunneling Microscopy*, Vol. 227 (Oxford University Press, New York/Oxford, 1993).
[21] The comparison between dI/dV and $(dI/dV)/(I/V)$ curves demonstrates that any artifacts are not induced by the normalization process except for small energy shifts toward E_F less than 40 meV. The scattered intensity in the Mott gap stems from the enhanced noise due to zero denominator.
[22] J.-J. Kim, I. Ekvall, and H. Olin, Phys. Rev. B **54**, 2244 (1996).
[23] L. Perfetti *et al.*, New J. Phys. **10**, 053019 (2008).
[24] F. Zwick, H. Berger, I. Vobornik, G. Margaritondo, L. Forró, C. Beeli, M. Onellion, G. Panaccione, A. Taleb-Ibrahimi, and M. Grioni, Phys. Rev. Lett. **81**, 1058 (1998).
[25] X.-L. Yu *et al.*, arXiv:1407.1407.
[26] P. Darancet, A. J. Millis, and C. A. Marianetti, Phys. Rev. B **90**, 045134 (2014).
[27] C. Arguello *et al.*, Phys. Rev. B **89**, 235115 (2014).
[28] P. Mallet, K. M. Zimmermann, Ph. Chevalier, J. Marcus, J. Y. Veuillen, and J. M. Gomez Rodriguez, Phys. Rev. B **60**, 2122 (1999).
[29] P. Mallet, H. Guyot, J. Y. Veuillen, and N. Motta, Phys. Rev. B **63**, 165428 (2001).
[30] S. J. Park *et al.*, Phys. Rev. Lett. **93**, 106402 (2004).
[31] K. C. Rahnejat *et al.*, Nat. Commun. **2**, 558 (2011).
[32] J. Dai, Eduardo Calleja, Jacob Alldredge, Xiangde Zhu, Lijun Li, Wenjian Lu, Yuping Sun, Thomas Wolf, Helmuth Berger, and Kyle McElroy, Phys. Rev. B **89**, 165140 (2014).
[33] K. Rossnagel and N. V. Smith, Phys. Rev. B **73**, 073106 (2006).
[34] C. Sohrt, A. Stange, M. Bauer, and K. Rossnagel, Faraday Discuss. **171**, 243 (2014).
[35] P. Xu, J. O. Piatek, P.-H. Lin, B. Sipos, H. Berger, L. Forró, H. M. Rønnow, and M. Grioni, Phys. Rev. B **81**, 172503 (2010).
[36] P. J. H. Denteneer, R. T. Scalettar, and N. Trivedi, Phys. Rev. Lett. **87**, 146401 (2001).
[37] H. Eskes, M. B. J. Meinders, and G. A. Sawatzky, Phys. Rev. Lett. **67**, 1035 (1991).
[38] M. Imada, A. Fujimori, and Y. Tokura, Rev. Mod. Phys. **70**, 1039 (1998).
[39] Y. Okada *et al.*, Nat. Mater. **12**, 707 (2013).
[40] C. Ye *et al.*, Nat. Commun. **4**, 1365 (2013).
[41] W.-H. Leong, S.-L. Yu, T. Xiang, and J.-X. Li, Phys. Rev. B **90**, 245102 (2014).
[42] E. Berger, P. Valášek, and W. von der Linden, Phys. Rev. B **52**, 4806 (1995).